Eur. Phys. J. D **21**, 63–71 (2002)
DOI: 10.1140/epjd/e2002-00178-y

THE EUROPEAN PHYSICAL JOURNAL D

Nonlinear Hanle effect in Cs vapor under strong laser excitation

A.V. Papoyan[1,a], M. Auzinsh[2], and K. Bergmann[3]

[1] Institute for Physical Research, NAS of Armenia, Ashtarak-2 378410, Armenia
[2] Department of Physics, University of Latvia, 19 Rainis boulevard, Riga 1586, Latvia
[3] Fachbereich Physik, Universität Kaiserslautern, 67653 Kaiserslautern, Germany

Received 24 November 2001 / Received in final form 25 March 2002
Published online 24 September 2002 –

Abstract. We report results of a theoretical and experimental study of the ground state nonlinear Hanle effect under strong laser excitation. It is shown that besides the well-known zero-magnetic field suppression of absorption on $F_g = F \longrightarrow F_e = F - 1$ transitions caused by population trapping, an optical pumping induced enhanced absorption occurs on $F_g = F \longrightarrow F_e = F + 1$ transitions for small B-fields. The latter effect becomes more pronounced for high F values. The experiment with atomic vapor of Cs (D_2 line, $F_g = 4$) confirms an increase of the spectrally unresolved fluorescence yield at zero magnetic field and 600 mW/cm^2 laser intensity by 9% or 42%, when excitation occurs with linearly or circularly polarized light, respectively. The results of the experiment agree with numerical simulation studies using equations of motion for a density matrix.

PACS. 32.80.Bx Level crossing and optical pumping – 32.80.Qk Coherent control of atomic interactions with photons – 42.50.Gy Effects of atomic coherence on propagation, absorption, and amplification of light

1 Introduction

Optical pumping and laser-induced atomic coherences may significantly alter the intensity, polarization and spatial distribution of the laser-induced fluorescence of atoms. A well-known manifestation of coherence phenomenon in atoms is the linear Hanle effect [1,2] observable under weak coherent optical excitation of magnetic sublevels in an external magnetic field. In case of nonlinear light absorption one of the most interesting effects is coherent population trapping. Coherent population trapping (CPT) was first experimentally observed in 1976 in the interaction of sodium atoms with a laser field [3]. In CPT destructive quantum interference between different excitation pathways causes the trapping of population in a coherent superposition of ground state sublevels. Once established such a superposition, a dark state [4], is immune against further radiative interaction. As a result fluorescence from an ensemble of atoms decreases, while the intensity of the transmitted light increases. An external magnetic field **B** perpendicularly to the light polarization **E** destroys the coherence between ground state sublevels.

Coherence in an atomic ground state is the basis of *e.g.* lasing without inversion [5], new schemes for magnetometry [6] or laser cooling [7], electromagnetically induced transparency [8] and the very recent work on coherent information storage using halted light pulses [9,10]. Those applications triggered detail studies of dark resonances, including open systems [11] and systems with losses [12]. In the course of these studies, a new phenomenon was observed by the authors of [13]. In that work ^{85}Rb atoms were excited to the $5P_{3/2}$ states by a diode laser from the $F_g = 3$ hyperfine level of the ground $5S_{1/2}$ state. The Doppler-broadening prevented the resolution of hyperfine components of the excited state. All dipole allowed transitions to the electronically excited state with excited state quantum numbers $F_e = 2$, 3, and 4 were excited simultaneously. However, atoms excited to different hyperfine levels are associated with different velocity classes. Contrary to the usual reaction of a dark resonance signal to a B-field the authors of the paper [13] observed an increase of transmittance and a decrease of fluorescence intensity when a magnetic field was applied. For excitation with linearly or circularly polarized laser radiation tuned to D_1 and D_2 lines, subnatural-width resonances were observed in [14].

This phenomenon was discussed in several recent papers [14–17]. In [15,16] Arimondo and coworkers analyzed the enhanced absorption for the case that $F_g < F_e$ in the Hanle configuration (with a single laser field applied to an atomic transition, and the Zeeman degeneracy in the lower and upper states broken by an applied magnetic field). In [17] a simple explanation of the enhanced absorption for $B = 0$ and the transition $F_g = F \rightarrow F_e = F + 1$ was presented. The effect was also observed experimentally in D_2 line absorption in Rb vapor [17].

[a] e-mail: papoyan@ipr.sci.am

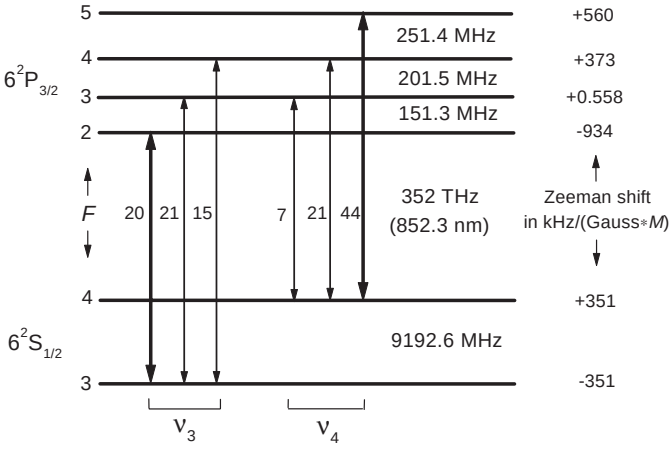

Fig. 1. Relevant energy levels and hyperfine transitions for Cs D_2 line including relative transition probabilities.

The phenomena in external magnetic field as described above, is rather similar to the effect of electromagnetically induced absorption analyzed and measured in Rb atoms in [18,19]. The authors of the latter papers analyze the absorption of a weak probe field as a function of its detuning from the frequency of the strong pump field for $B = 0$. A strong enhancement of the absorption was observed for $F_g = F \rightarrow F_e = F + 1$ when frequencies of the pump and probe fields coincide.

In the present work, we study experimentally and theoretically the total intensity of the fluorescence as observed at a specific direction at the two spectrally resolved groups of the hyperfine transitions of Cs D_2 line: $F_g = 3 \longrightarrow F_e = 2, 3, 4$ and $F_g = 4 \longrightarrow F_e = 3, 4, 5$ (Fig. 1) for excitation with linear or circular polarized light. When pumping occurs with intense laser fields (up to 600 mW/cm^2) new features of the magneto-optical response of Cs vapor are observed. For several experimental situations an increase of the fluorescence intensity at zero magnetic field was observed. We explain these dip and peak structures in terms of a semi quantitative as well as in a more exact numerical model involving modification of the total absorption caused by optical pumping and the creation of coherences among magnetic sublevels of the hyperfine states, with the magnetic field restricted to the range of the linear Zeeman effect.

2 Experimental

The experimental setup is schematically shown in Figure 2. The continuous radiation of a titanium:sapphire laser is directed unfocused (beam diameter 2 mm) into the 1.65 cm-long all-sapphire cell with the side-arm containing cesium. The cell diameter is 1.5 cm; no buffer gas has been added when sealing the cell. The cell windows (flat and parallel) were cut normal to the c-axis to avoid birefringence. For the cell inserted between the crossed polarizers, the measured extinction ratio was $\sim 10^{-5}$ (10^{-6} without the cell). The temperature of the

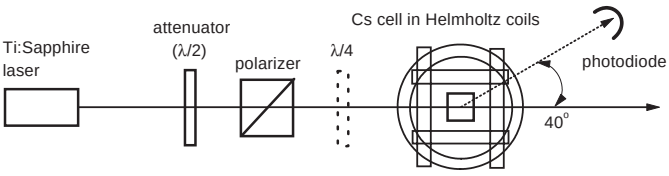

Fig. 2. The experimental setup (schematic).

side-arm was controlled by a Peltier element and stabilized to $\Delta T = 0.05$ °C accuracy with active feedback. In all the measurements, the side-arm temperature was kept at 20 °C which corresponds to a number density of atoms of $N = 2.8 \times 10^{10}$ cm^{-3}.

The photodiode which detects the fluorescence from the vapor is placed at an angle of 40° relative to the laser beam, in the horizontal plane perpendicular to the initial (vertical) laser polarization[1]. The signal from the photodiode is amplified and recorded by a Tektronix TDS 340A digital oscilloscope operated in the averaging mode, followed by computer data processing. A second photodiode (not shown) monitors the laser beam intensity transmitted through the cell.

The fluorescence and transmission spectra are recorded by scanning the frequency of the laser radiation over a range of typically $\Delta\nu_{\rm scan} = 2$ GHz (maximum $\Delta\nu_{\rm scan} = 20$ GHz), around the D_2 line of Cs atoms ($\lambda = 852.3$ nm). The typical duration of one scan was $T_{\rm scan} = 0.25$ s which is long enough to allow steady-state conditions to develop. Indeed, even for the largest value of $\Delta\nu_{\rm scan}$, the time needed to sweep across the homogeneous linewidth,

$$\frac{\Gamma \times T_{\rm scan}}{2\pi\Delta\nu_{\rm scan}} = 7.5 \times 10^{-5} \text{ s} \qquad (1)$$

(Γ is a spontaneous relaxation rate of the excited state) is larger than the shortest time of flight ($\Delta t_{\rm tof} = 9 \times 10^{-6}$ s) for atoms travelling at the mean velocity across the laser beam with diameter of 2 mm. Furthermore $\Delta t_{\rm tof}$ is much larger than the radiative decay time of the excited levels. No spectral analysis of the emitted radiation was done in the present experiment.

The laser power delivered to the setup by a single-mode optical fiber was about 300 mW which corresponds to $I_{\rm L} = 9.6$ W/cm^2 maximum radiation intensity at the cell entrance. The spectral width of the laser radiation was about 1 MHz. A Glan-Thomson prism was used to reduce the impurity of linear polarization of the laser radiation to $< 10^{-6}$. An adjustable $\lambda/4$ plate was inserted when circular laser polarization was needed.

The ambient laboratory magnetic field was compensated in all directions by a set of 3 orthogonal pairs of Helmholtz coils. The magnetic field in the region of the Cs cell was monitored by a digital teslameter with the

[1] The exact angular position of the photodiode is not important for the current study. The value of 40° was chosen because of convenience with regard to the geometric constraints imposed by the mounting elements of the cell and the Helmholtz coils. The given observation angle is taken into account for the simulation of the experimental signals (Sect. 6).

accuracy of 0.05 gauss. The coils where also used to apply a magnetic field of up to 80 gauss.

Since the hyperfine splitting of the $6P_{3/2}$ level is less than the Doppler broadening (~ 380 MHz), only two spectrally resolved lines were recorded: $6S_{1/2}$, $F_g = 3 \longrightarrow 6P_{3/2}$, $F_e = 2, 3, 4$ (ν_3) and $6S_{1/2}$, $F_g = 4 \longrightarrow 6P_{3/2}$, $F_e = 3, 4, 5$ (ν_4), see Figure 1. The frequency separation of these lines is given by the hyperfine splitting of the $6S_{1/2}(F = 3, 4)$ ground state, $\Delta\nu_{\rm HFS} = 9.2$ GHz.

An auxiliary saturated absorption setup (not shown) with a separate reference Cs cell allowed the precise frequency scaling in the D_2 line region using the hyperfine transitions and crossover resonances with a linewidth $\Delta\nu < 10$ MHz. The signal from this setup was recorded simultaneously with the fluorescence signal.

We have studied the dependence of the spectrally unresolved fluorescence of the ν_3 and ν_4 transitions on the strength of the magnetic field for excitation with of linearly- and circularly-polarized light, and for various orientations of the magnetic field.

3 Experimental results

Data is presented for different combinations of laser polarization and magnetic field orientation, and for two values of the incident laser intensity: $I_{\rm L} = 30$ mW/cm^2 and $I_{\rm L} = 600$ mW/cm^2. There was no detectable dependence of the fluorescence signal on the magnetic field at low laser intensity ($I_{\rm L} < 1$ mW/cm^2), independent of the B-field orientation and laser polarization.

We present results obtained in a configuration of laser polarization and magnetic field that allows coupling of magnetic sublevels. For excitation with laser radiation of linear polarization $\mathbf{E}$ the measured variation of the fluorescence signal with the magnetic field was qualitatively the same when the B-field was oriented either parallel to the direction of laser propagation $\mathbf{k}$ ($\mathbf{B} \parallel \mathbf{k}$, $\mathbf{B} \perp \mathbf{E}$) or perpendicular to $\mathbf{k}$ and $\mathbf{E}$ ($\mathbf{B} \perp \mathbf{k}$, $\mathbf{B} \perp \mathbf{E}$). For excitation with circular laser polarization the measured dependence of the fluorescence signal on magnetic field was qualitatively the same for any direction of B-field in the transverse plane ($\mathbf{B} \perp \mathbf{k}$).

Figure 3 shows a set of representative results (fluorescence intensity *vs.* strength of B-field). For the case of linear (vertical) laser polarization the B-field was directed along the wave vector $\mathbf{k}$, and for the case of circular polarization the B-field was directed vertically (perpendicular both to $\mathbf{k}$ and observation direction). The signal is given in arbitrary units but the scale of these units is the same for all four frames.

Each experimental point in Figure 3 represents a fluorescence signal integrated over the Doppler profile at given B value. The total fluorescence signal in a specific direction originates from resonant absorption of laser radiation by atoms. It reflects the total population of the excited state sublevels and coherences created among them. Only atoms from those velocity groups which are resonant with the scanning laser frequency (within the power broadened homogeneous linewidth) contribute to the absorption [20]. Sweeping the laser frequency across the Doppler profile allows the collection of the resonant fluorescence contribution from all the atoms, independently of their velocity. Hence, the dependence of the fluorescence on magnetic field is not affected by Doppler broadening. Indeed, the narrow and broad features that can be seen in Figure 3, are of sub-Doppler width.

When several hyperfine transitions overlap with the Doppler width, as in the present experiment, the contribution of individual transitions to the integral fluorescence is not resolved. Therefore, the variation of the intensity of the laser induced fluorescence with laser frequency does not yield useful information in the context of this experiment. Under conditions relevant for Figure 3 (high laser intensity) it is mainly the transitions $F_g = 3 \longrightarrow F_e = 2$ for ν_3 and $F_g = 4 \longrightarrow F_e = 5$ for ν_4 which contribute to the signal. Atoms which absorb photons on the so-called open transitions $F_g = 3 \longrightarrow F_e = 3, 4$ and $F_g = 4 \longrightarrow F_e = 3, 4$ eventually spontaneously decay to the non-absorbing ground sublevel $F_g = 4$ and $F_g = 3$, respectively, and are lost. Therefore, the integral fluorescence signal, shown in Figure 3, is proportional to the corresponding intensity of the cycling transition.

3.1 Results for the ν_3 line

With linear laser polarization we observe for the ν_3 line a minimum of the fluorescence intensity for $B = 0$, at low and high laser intensity $I_{\rm L}$ (lower graphs in Figs. 3a and 3b). This observation is a manifestation of population trapping among the magnetic substates of the ground state hyperfine level. Since the population trapping is intrinsically a single-atom process, Doppler-broadening is not detrimental. The width and depth of the structure are not sensitive to the atomic velocity.

In the limit of low pumping intensity, the width of the fluorescence dip is determined by the interaction time (time of flight through the laser beam). At higher intensities power broadening is observable. Figure 4 shows the intensity dependence of the contrast and width of a dip. The contrast is defined as $(\mathcal{F}(B_{\rm max}) - \mathcal{F}(0))/\mathcal{F}(B_{\rm max})$ where $\mathcal{F}(0)$ is a fluorescence signal at $B = 0$, and $\mathcal{F}(B_{\rm max})$ is the maximum fluorescence signal for the whole B-field range. The width of the dip as a function of the B-field is defined as a full width of a fluorescence signal at the level of $0.5\,(\mathcal{F}(B_{\rm max}) + \mathcal{F}(0))$. After an initial rapid increase with $I_{\rm L}$, no further increase of the contrast beyond the level of 62% is found. This observation is in qualitative agreement with results reported in [12].

Results for excitation with circular laser polarization are shown in Figures 3c and 3d. Here the magnetic field direction is perpendicular to the laser propagation $\mathbf{k}$ (transverse field). The width of a fluorescence dip in this case is nearly the same as for excitation with linear polarization. The maximum contrast is somewhat higher (64%).

3.2 Results for the ν_4 line

For the ν_4 line ($F_g = 4 \longrightarrow F_e = 3, 4, 5$), a central peak develops at $B = 0$ except for linear polarization and

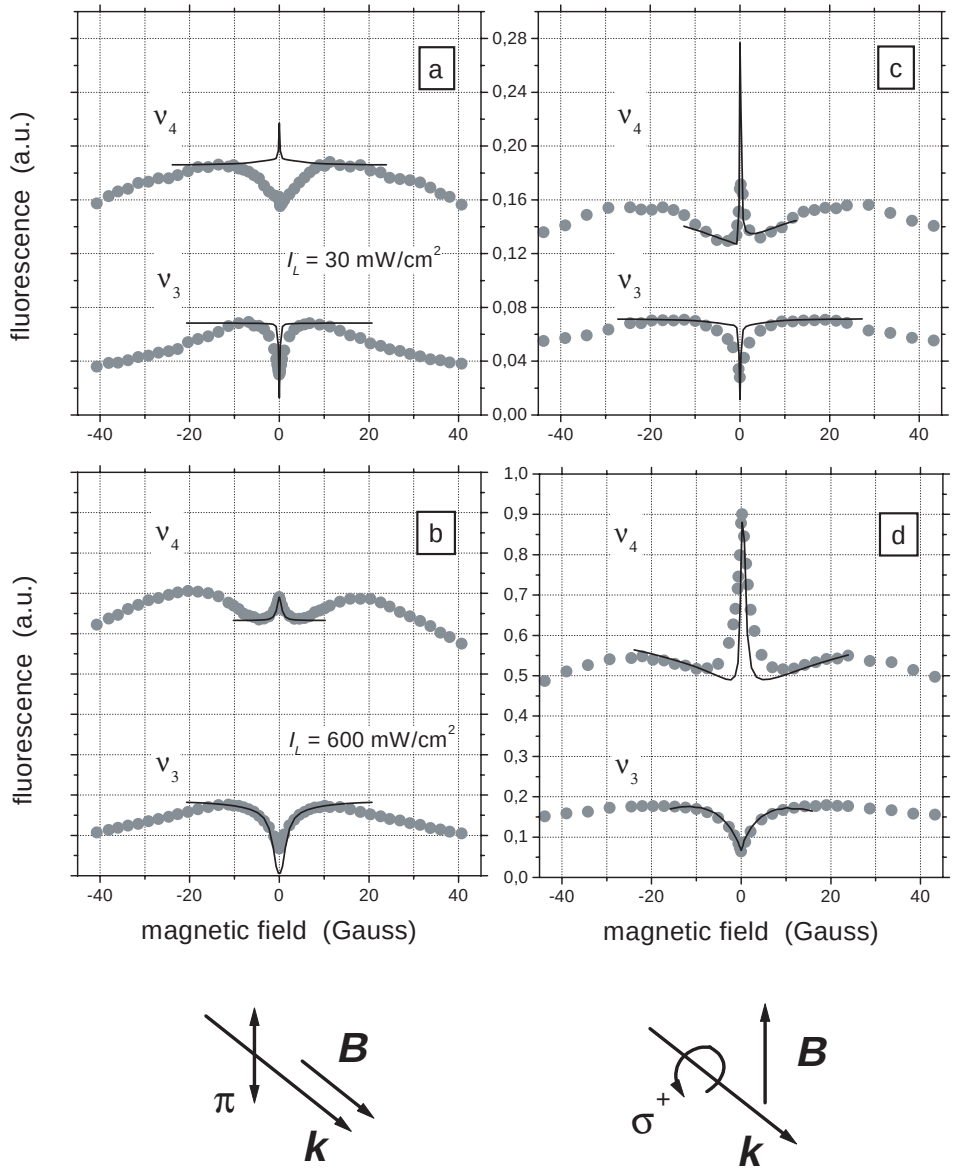

Fig. 3. Variation of the integral fluorescence with the magnetic field for excitation with linear (a, b) and circular (c, d) laser polarization. Circles: experiment, solid lines: simulation. The laser intensities are: 30 mW/cm^2 for (a) and (c) and 600 mW/cm^2 for (b) and (d). The relative orientation of laser polarization with respect to the direction of laser propagation **k** and magnetic field **B** is shown below the graphs. The signals are given in arbitrary units but the normalization factor is the same for all the graphs. The fit parameter Γ_p (units of 10^{-6} s^{-1}) is for (a) and (c) $\Gamma_p = 4.5$ (ν_3) and $\Gamma_p = 10$ (ν_4), and $\Gamma_p = 91$ (ν_3) and $\Gamma_p = 250$ (ν_4) for (b) and (d).

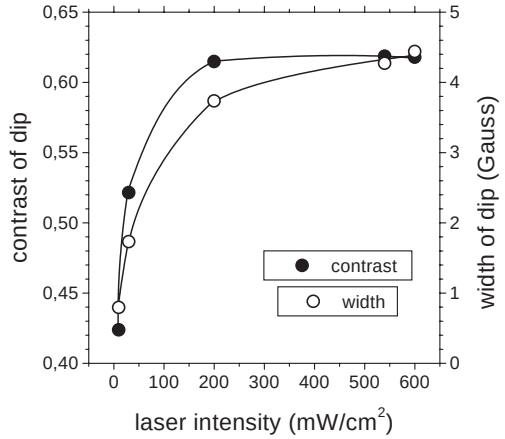

Fig. 4. Contrast and full width at half maximum of the structure for the ν_3 line as a function of the laser intensity for linear polarization. The solid lines are shown to guide the eye.

$I_{\rm L} = 30$ mW/cm^2. The magnitude of a fluorescence peak is much larger for circularly polarized excitation than for linear polarization. The appearance of the $B = 0$ peak is a result of more subtle and less intuitive effect compared with the population trapping which causes the $B = 0$ dip for ν_3 line. The physical mechanism responsible for this peak is discussed in Section 4.

The steady-state contribution to the fluorescence arises mainly from those atoms that absorb photons on the cycling transition $F_g = 4 \longrightarrow F_e = 5$ (this transition is neither affected by depopulation pumping, nor by population trapping). Nevertheless, there is a consequence of the non-negligible contribution from the non-cycling transitions. In all cases (low and high laser intensity, linear and circular polarization), the fluorescence intensity tends to decrease as $B \to 0$. This feature can be understood by involving transient population trapping on the "open" transitions $F_g = 4 \longrightarrow F_e = 3, 4$ [12].

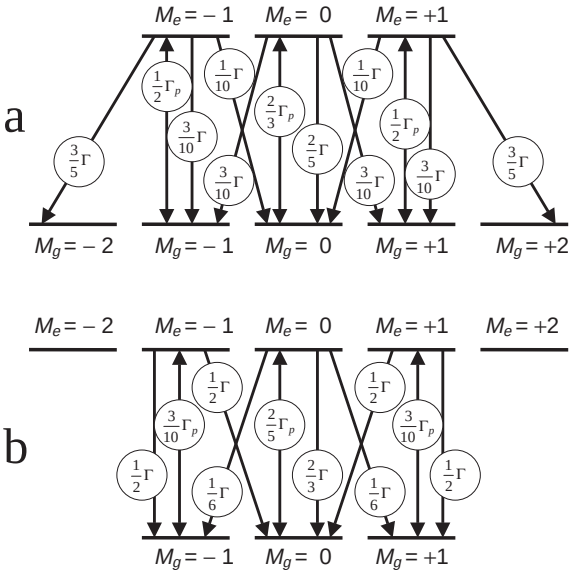

Fig. 5. Transitions between magnetic sublevels and their relative rates for $F_g = 2 \longleftrightarrow F_e = 1$ (a) and $F_g = 1 \longleftrightarrow F_e = 2$ (b) transitions, with linearly polarized excitation light.

Although the $F_g = 4$ state is depopulated by optical pumping for those atoms which absorb radiation on noncycling transitions, the absorption does not vanish because of the permanent influx of unexcited atoms into the laser beam. Moreover, the optically pumped atoms departing from the interaction region may undergo spin exchange collisions with the cell walls [21], resulting in repopulation of the absorbing ground sublevel.

This supposition is supported by the following experimental observation. As $I_{\rm L}$ increases towards the maximum value, we observe a continuous decrease (but not complete suppression) of the fluorescence signal normalized to the laser intensity in the spectral region of $F_g = 4 \longrightarrow F_e = 3, 4$ transitions. Accordingly, the mentioned dip in a total fluorescence signal, on which the $B \approx 0$ peak is superimposed, is somewhat larger for $I_{\rm L} = 30$ mW/cm^2 ($\sim$15%) compared to $I_{\rm L} = 600$ mW/cm^2 ($\sim$7%).

4 Qualitative model: ground state Hanle effect

We begin with a qualitative consideration of the circumstances under which a decrease or an increase of the fluorescence or transmittances is observed in a coherently driven medium when a magnetic field B is reduced to zero.

When only one optical field is present the traditional dark resonance is associated with optical pumping [4,22]. We consider the excitation of an atomic transition $F_g = 2 \longrightarrow F_e = 1$ with a linearly polarized light. The direction of the quantization axis is chosen along the electric field vector **E**. Transitions occur between magnetic sublevels with $\Delta M = M_g - M_e = 0$ (see Fig. 5a). Absorption does not occur from $M_g = \pm 2$. These selection rules reflect the axial symmetry of the excitation process. Spontaneous decay is a spatially isotropic process subject to the selection rules $\Delta M = 0, \pm 1$ for electric dipole transitions. This means that two of the excited state magnetic sublevels, namely $M_e = \pm 1$ decay to the nonabsorptive ground state sublevels $M_g = \pm 2$. If the relaxation in the ground state is slow compared to the rate of excitation, most of the population will be optically pumped to the $M_g = \pm 2$ sublevels and will be trapped there. As a result the fluorescence intensity decreases and the transmittance increases as the steady state condition is approached. Application of an external magnetic field in a direction perpendicular to **E** leads to Larmor precession and thus to mixing of ground state magnetic sublevels. As a result absorption and fluorescence intensity will increase with B.

A similar reasoning explains the increase of the fluorescence for $B \to 0$, as first reported in [23] and analyzed in [14–17]. When the excitation occurs on the atomic transition $F_g = 1 \longrightarrow F_e = 2$ (*i.e.* $F_e > F_g$) in the same geometry as in the previous example all magnetic sublevels absorb light. There are no sublevels that trap population and, as shown for example in [4], dark resonances do not appear. Here, the magnetic field induces a redistribution of population with the consequence that, on average, the excitation probability is smaller for $B \neq 0$.

The absorption rates between respective magnetic sublevels for linearly polarized π absorption is given by [24]

$$\Gamma_{M_g \to M_e} = \Gamma_p \frac{2F_g + 1}{2F_e + 1} \left(C^{F_e M_e}_{F_g M_g 10} \right)^2 , \qquad (2)$$

where Γ_p is the absorption rate and the $C^{c\gamma}_{a\alpha b\beta}$ are the respective Clebsch–Gordan coefficients. The rate of spontaneous transitions between excited and ground state magnetic sublevels, is

$$\Gamma_{M_e \to M_g} = \Gamma \frac{2F_e + 1}{2F_g + 1} \left(C^{F_g M_g}_{F_e M_e 1 M_g - M_e} \right)^2 , \qquad (3)$$

where Γ is a spontaneous relaxation rate of the excited state. The relative transition rates between magnetic sublevels of $F_g = 1 \longleftrightarrow F_e = 2$ transition are shown in Figure 5b. The magnetic sublevel $M_g = 0$ is the most absorbing state. Furthermore, spontaneous emission from the excited states predominantly reaches the $M_g = 0$ sublevel. Thus, optical pumping drives the atom into the strongly absorbing state. An external magnetic field perpendicularly to the z-axis, redistributes population between ground state magnetic sublevels. Consequently the population of less absorbing magnetic sublevels $M_g = \pm 1$ will increase. Therefore the total absorption and fluorescence intensity will decrease and the transmittance will increase with increasing B.

These qualitative considerations are substantiated by solving balance equations for the stationary population n_{M_g} and n_{M_e} of magnetic sublevels. Disregarding decay to other hyperfine levels of the ground state, the steady state population of the magnetic sublevels when the $F_g = 1 \to F_e = 2$ transition is driven by linearly polarized light

is – for the ground state

$$ {}^{g}n_{-1} = \frac{6(10\Gamma + 3\Gamma_p)}{5(17\Gamma + 12\Gamma_p)}\,\overline{n_g}, \qquad {}^{g}n_{0} = \frac{27(5\Gamma + 2\Gamma_p)}{5(17\Gamma + 12\Gamma_p)}\,\overline{n_g}, $$
$$ {}^{g}n_{+1} = \frac{6(10\Gamma + 3\Gamma_p)}{5(17\Gamma + 12\Gamma_p)}\,\overline{n_g}, \tag{4} $$

and for the excited state

$$ {}^{e}n_{-2} = 0, \qquad {}^{e}n_{-1} = \frac{18\Gamma_p}{5(17\Gamma + 12\Gamma_p)}\,\overline{n_g}, $$
$$ {}^{e}n_{0} = \frac{54\Gamma_p}{5(17\Gamma + 12\Gamma_p)}\,\overline{n_g}, $$
$$ {}^{e}n_{+1} = \frac{18\Gamma_p}{5(17\Gamma + 12\Gamma_p)}\,\overline{n_g}, \qquad {}^{e}n_{+2} = 0 \tag{5} $$

where $\overline{n_g}$ is the average ground state magnetic sublevel population in absence of the radiation. In the limit of weak absorption, $\Gamma_p \ll \Gamma$, we have

$$ {}^{g}n_{-1} \approx \frac{12}{17}\overline{n_g} \approx 0.706\ \overline{n_g}, \quad {}^{g}n_{0} \approx \frac{27}{17}\overline{n_g} \approx 1.59\ \overline{n_g}, $$
$$ {}^{g}n_{+1} \approx \frac{12}{17}\overline{n_g} \approx 0.706\ \overline{n_g}, \quad {}^{e}n_{i} \equiv 0. \tag{6} $$

while for strong saturation, $\Gamma_p \gg \Gamma$, we find

$$ {}^{e}n_{-2} \equiv 0, \qquad {}^{e}n_{-1} \approx {}^{g}n_{-1} \to \frac{3}{10}\overline{n_g} = 0.3\ \overline{n_g}, $$
$$ {}^{e}n_{0} \approx {}^{g}n_{0} \to \frac{9}{10}\overline{n_g} = 0.9\ \overline{n_g}, $$
$$ {}^{e}n_{+1} \approx {}^{g}n_{+1} \to \frac{3}{10}\overline{n_g} = 0.3\ \overline{n_g}, \qquad {}^{e}n_{+2} \equiv 0. \tag{7} $$

This type of $F \to F{+}1$ optical pumping was first discussed in [23], but did not receive much attention. Recently it was analyzed in [15–17,25].

The increase of the overall absorption over the absorption from an ensemble with equally populated magnetic sublevels is given by

$$ \Delta A = \frac{\sum_{M_g=-F_g}^{F_g}\sum_{M_e=-F_e}^{F_e}(n_{M_g} - n_{Me})\Gamma_{M_g\to M_e}}{\sum_{M_g=-F_g}^{F_g}\sum_{M_e=-F_e}^{F_e}(\overline{n_{M_g}} - \overline{n_{Me}})\Gamma_{M_g\to M_e}} \tag{8} $$

with $\overline{n_{M_g}} = \sum n_{M_g}/(2F_g+1)$ and $\overline{n_{Me}} = \sum n_{Me}/(2F_e+1)$. For excitation with light of arbitrary intensity, equation (8) yields $\Delta A = 18/17 \approx 1.059$ (5.9%).

The results of a similar analysis for the transition $F_g = 4 \longrightarrow F_e = 5$, relevant for our experiments with Cs are shown in a Figure 6. As expected, for $B = 0$, the population of magnetic sublevels is driven to the most absorbing magnetic sublevels with small magnetic quantum numbers.

It is straightforward to extend this analysis to excitation with circularly polarized light. With respect to a quantization axis along the laser beam direction the selection rule for the absorption process is $\Delta M = M_g - M_e = \pm 1$.

When the excitation occurs on the atomic transition $F_g = F \longrightarrow F_e = F - 1$, all the population is driven by optical pumping into $M_g = F, F{-}1$ or $M_g = -F, -(F{-}1)$ states (depending on the helicity of the light) where it is trapped when $B = 0$. For $B \neq 0$ Larmor precession prevents the trapping.

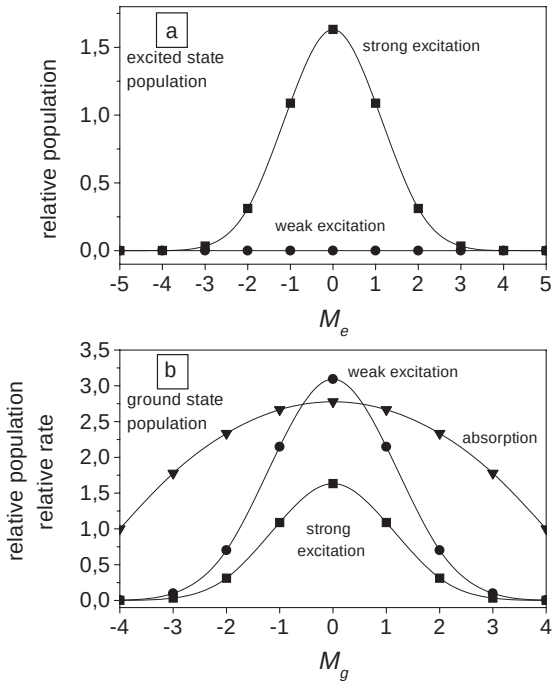

Fig. 6. Steady state population distribution over magnetic sublevels M_i for $F_g = 4 \longrightarrow F_e = 5$ transition excited by linearly polarized light. (a) Results for electronically excited state, (b) results for the electronic ground state. The triangles show the relative rate of absorption for $M_g \longrightarrow M_e = M_g$ transitions. The solid lines are shown to guide the eye.

For the excitation on the atomic transition $F_g = F \longrightarrow F_e = F{+}1$, even in the limit of weak excitation the ground state population is driven by optical pumping to one of the sublevels $M_g = \pm F_g$ depending on the sense of circular polarization. These sublevels are those with the strongest absorption, given by

$$ \Gamma_{M_g\to M_e} = \Gamma_p \frac{2F_g+1}{2F_e+1}\left(C^{F_e M_e}_{F_g M_g 1\pm 1}\right)^2. \tag{9} $$

The optical pumping induces an increase ΔA of the absorption of circularly polarized light for a transition $F_g \to F_e = F_g + 1$ over the case of equally populated sublevels M_g, by

$$ \Delta A = \frac{3(2F_g+1)}{2F_g+3}\,. \tag{10} $$

That analytic result is correct for excitation of arbitrary intensity. The variation of ΔA with F_g is shown in Figure 7 for excitation of any strength with linearly and circularly polarized light.

A similar analysis has been presented by Taichenachev *et al.* [25] for zero magnetic field and in the limit of low laser intensity. Those authors show that, for a given laser

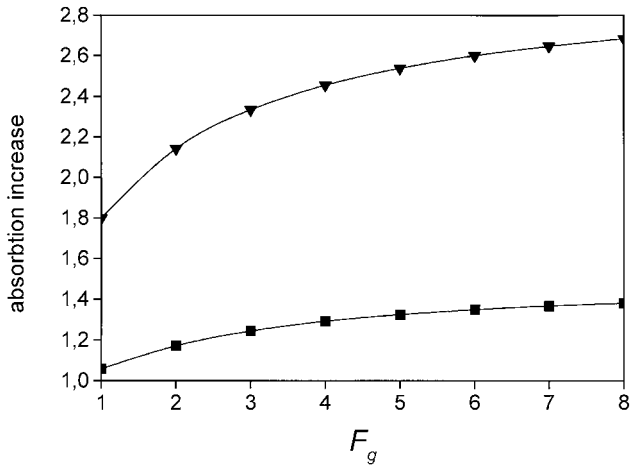

Fig. 7. Increase of absorption due to the redistribution of the population of ground state magnetic sublevels by optical pumping for a $F_g \longrightarrow F_e = F_g + 1$ transition for excitation of arbitrary strength. Triangles: excitation with circular laser polarization; squares: excitation with linear laser polarization. The solid lines are shown to guide the eye.

intensity, the steady state total absorption and hence, fluorescence intensity, is reduced or enhanced for linear or circular polarization, respectively, compared to an atomic gas with uniform population of magnetic sublevels. As the intensity increase towards the saturation regime, the dependence of the absorption coefficient on polarization becomes weaker and eventually vanishes.

The discussion presented above provides insight into the consequences of optical pumping for the total absorption but is qualitative in the sense that it does not allow to predict the shape and width of the structure as the strength of B-field is varied. A quantitative description of the phenomenon requires the solution of the density matrix equations for an open system with losses, discussed in the following section.

5 Extended model: density matrix calculations

More elaborate numerical simulation of the experiment requires the integration of the density matrix equations. The code was written under the assumption of broad spectral line excitation [26]. That assumption is justified, since the laser frequency is continuously scanned over a range of several GHz. Furthermore, the hyperfine splitting of the states $F_e = 3, 4$, and 5 for the ν_4 transition and $F_e = 2, 3$, and 4 for the ν_3 transition is larger than the homogeneous linewidth. Therefore, for a given laser frequency each $F_g \rightarrow F_e$ transition is associated with a different velocity class. Thus, the various $F_g \rightarrow F_e$ transitions are not coupled but driven independently. In previous works, a broad line excitation model in laser experiments with atoms [17,27] and molecules [26] proved to give very good results.

The equations of motion for the density matrix read

$$\dot{f}_{M_e M'_e} = \Gamma_p \sum_{M_g M'_g} \langle M_e | \mathbf{E}^\star \mathbf{d} | M_g \rangle \langle M'_e | \mathbf{E}^\star \mathbf{d} \left| M'_g \right\rangle^\star \varphi_{M_g M'_g} - \left(\frac{\Gamma_p}{2} + \mathrm{i}\omega_\mathrm{S} \right) \sum_{M''_e M_g} \langle M_e | \mathbf{E}^\star \mathbf{d} | M_g \rangle \left\langle M''_e \right| \mathbf{E}^\star \mathbf{d} | M_g \rangle^\star f_{M''_e M'_e} - \left(\frac{\Gamma_p}{2} - \mathrm{i}\omega_\mathrm{S} \right) \sum_{M''_e M_g} \left\langle M''_e \right| \mathbf{E}^\star \mathbf{d} | M_g \rangle \left\langle M'_e \right| \mathbf{E}^\star \mathbf{d} | M_g \rangle^\star f_{M_e M''_e} - \Gamma f_{M_e M'_e} - \mathrm{i}\omega_{M_e M'_e} f_{M_e M'_e} \quad (11)$$

$$\dot{\varphi}_{M_g M'_g} = -\left(\frac{\Gamma_p}{2} + \mathrm{i}\omega_\mathrm{S} \right) \sum_{M''_g M_e} \langle M_g | \mathbf{E}^\star \mathbf{d} | M_e \rangle \left\langle M''_g \right| \mathbf{E}^\star \mathbf{d} | M_e \rangle^\star \times \varphi_{M''_g M'_g} - \left(\frac{\Gamma_p}{2} - \mathrm{i}\omega_\mathrm{S} \right) \sum_{M''_g M_e} \left\langle M''_g \right| \mathbf{E}^\star \mathbf{d} | M_e \rangle \left\langle M'_g \right| \mathbf{E}^\star \mathbf{d} | M_e \rangle^\star \times \varphi_{M_g M''_g} + \Gamma_p \sum_{M_e M'_e} \langle M_g | \mathbf{E}^\star \mathbf{d} | M_e \rangle \left\langle M'_g \right| \mathbf{E}^\star \mathbf{d} | M'_e \rangle^\star f_{M_e M'_e} - \gamma \varphi_{M_g M'_g} - \mathrm{i}\omega_{M_g M'_g} \varphi_{M_g M'_g} + \sum_{M_e M'_e} \Gamma^{M_e M'_e}_{M_g M'_g} f_{M_e M'_e} + \lambda \delta_{M_g M'_g} \quad (12)$$

where by $f_{M_e M'_e}$ and $\varphi_{M_g M'_g}$ are the density matrices of an excited and ground state level respectively. The first term on the right-hand side of equation (11) describes the absorption of light at rate Γ_p. The transition matrix elements of the form $\langle M_e | \mathbf{E}^\star \mathbf{d} | M_g \rangle$ account for the conservation of angular momentum during photon absorption with $\mathbf{E}$ being the polarization vector. The second and the third terms describe the stimulated emission of the light and the dynamic Stark shift ω_S. The fourth term characterizes the relaxation of the density matrix $f_{M_e M'_e}$ with a rate constant Γ. Finally, the fifth term describes the Zeeman splitting of the magnetic sublevels M_e and M'_e by a value of $\omega_{M_e M'_e} = (E_{M_e} - E_{M_{e'}})/\hbar$.

The first and the second terms on the right-hand side of equation (12) describe light absorption and the dynamic Stark shift, the third term the stimulated light emission, the fourth term the relaxation processes in the ground state, the fifth term the Zeeman interaction, the sixth term the repopulation by spontaneous transitions at a rate $\Gamma^{M_e M'_e}_{M_g M'_g}$, and the seventh term the relaxation of the density matrix of the ground state atoms interacting with the gas in a cell, not influenced by the radiation.

The matrix elements of electric dipole transition $\langle M_e | \mathbf{E}^\star \mathbf{d} | M_g \rangle$ is expanded as

$$\langle M_e | \mathbf{E}^\star \mathbf{d} | M_g \rangle = \sum_q (E^q)^* \langle M_e | d^q | M_g \rangle , \quad (13)$$

where the superscript q denotes the cyclic components of the respective vectors. The matrix elements at the r.h.s. of

equation (13) are further expanded, applying the Wigner–Eckart theorem, as

$$\langle M_e|\, d^q\, |M_g\rangle = \frac{1}{\sqrt{2F_e+1}} C^{F_e M_e}_{F_g M_g 1q} (F_e \,\|d\|\, F_g), \qquad (14)$$

where $(F_e \,\|d\|\, F_g)$ is the reduced matrix element. Under conditions of stationary excitation the system of equations (11, 12) becomes a system of linear equations for the ground and excited state density matrix elements. The coefficients of this system are calculated using angular momentum algebra and the formulas presented above. For further details see for example [26].

The analysis of the probabilities of optical transitions between hyperfine sublevels is based on the expression for relative transition rates between hyperfine states [28]

$$W_{F_g \to F_e} = (2F_e+1)(2F_g+1)(2J_e+1)(2J_g+1) \times \left\{ \begin{array}{ccc} J_g & F_g & I \\ F_e & J_e & 1 \end{array} \right\}^2 \left\{ \begin{array}{ccc} L_g & J_g & S \\ J_e & L_e & 1 \end{array} \right\}^2 . \qquad (15)$$

The level $F_e = 5$ is distinct from other excited state hyperfine levels since it decays only to the level $F_g = 4$. These two levels form a closed cycle for optical pumping [22] with no losses. All other levels of the excited state are part of an open system since population reaches both ground state hyperfine level $F_g = 3$ and 4 by spontaneous emission, with the relative rates given by equation (15).

Finally the fluorescence signal for each transition was calculated according to [26] from

$$I = \tilde{I}_o \sum_{M_e M'_e M_g} \langle M_e|(\mathbf{E}')^\star \mathbf{d}|M_g\rangle \langle M'_e|(\mathbf{E}')^\star \mathbf{d}|M_g\rangle^\star f_{M'_e M_e} \qquad (16)$$

where $\mathbf{E}'$ is a polarization of the observed light, while the coefficient $\tilde{I}_o$ includes all other factors such as the size of the solid angle from which the fluorescence is collected.

The signals are in some sense the same as expected for the ground state Hanle effect extensively studied in atoms and molecules, see for example [1,26,29–31].

6 Results of the simulation studies

The results of the simulation studies also shown in Figure 3 (solid lines) were obtained under the following assumptions and with the parameters given below:

- the calculation included the transition $F_g = 4 \leftrightarrow F_e = 5$ or $F_g = 3 \leftrightarrow F_e = 2$ of the ν_4 or ν_3 line, respectively;
- the Landé factors g_{F_i} of the ground and excited state hyperfine levels were calculated according to [2]

$$g_{F_i} = \frac{F(F+1)+J(J+1)-I(I+1)}{2F(F+1)} g_{J_i} - \frac{F(F+1)+I(I+1)-J(J+1)}{2F(F+1)} g_I,$$

where g_{J_i} and g_I are the electronic and nuclear Landé factors, respectively. The numerical values for the electronic and nuclear g-factors for Cs atom are [32] $g_{J_i}(6\mathrm{P}_{3/2}) = 1.3340(3)$, $g_{J_i}(6\mathrm{S}_{1/2}) = 2.00254032$ and $g_I = -0.00039885395(52)$;
- the relaxation rate of the excited state was taken as $\Gamma = 33 \times 10^6$ s^{-1} in all cases. This corresponds to a lifetime of $\tau = 29.8$ ns [33];
- the relaxation rate in the ground state, mainly determined by the thermal motion of atoms though the laser beam, is $\gamma = 0.1 \times 10^6$ s^{-1};
- in all cases the absorption rate Γ_p and an overall scaling factor I_o were used as fit parameters.

The simulation was done for the geometry as realized in the experiment. The variation of the magnetic field was restricted to the range of the linear Zeeman effect, *i.e.* B-field is too weak to cause uncoupling of the electronic angular momentum and nuclear spin.

The results of the simulation are shown as solid lines in Figure 3. The agreement of experimental and numerical results is good. Even the asymmetry of the structure (ν_4 signal circular polarization, Figs. 3c and 3d) around $B = 0$ is qualitatively represented. The reason for this asymmetry is the following. Excitation of atoms with a circularly polarized light creates an orientation along the direction $\mathbf{k}$ of the laser beam propagation. When transverse (vertical) magnetic field is applied, it causes a precession of this orientation in the observation plane (horizontal). The direction of the precession depends on sign of the applied B-field. Hence, for small enough $|B|$ values orientation is rotated towards the direction of the observation or away from it, resulting in some increase or decrease of the fluorescence signal (*i.e.*, asymmetry around $B = 0$).

Discrepancies between the results from the experiment and the simulations are caused by the restriction of the numerical studies to the cycling transitions, as well as by less than perfect accuracy of the measurement and incomplete compensation of the ambient magnetic field (in particular, *ac* components of the laboratory magnetic field have not been compensated). The resulting limitation in the B-field resolution is the most likely reason for the discrepancy of theory and experiment for the ν_4 lines, seen in Figure 3a. In the experiment, we do not observe the peak which is predicted by theory for $B = 0$. This predicted peak is the smallest and narrowest one among all the $B = 0$ features shown in Figure 3 and is thus most sensitive to small deviations of the experimental conditions assumed for the numerical calculations.

We restrict our signal simulation to magnetic field strength $B <$ 10–20 gauss. For larger magnetic field strength, the broad overall reduction of fluorescence seen in Figures 3a–3d, results from the fact that for $B >$ 10 gauss, the magnetic field decouples the electronic and nuclear spin in the electronically excited state of the atom, which leads to a mixing of hyperfine levels. Strict observation of selection rules with regard to transitions between F and M_F levels is essential to establish a cycling transition. Since F is no longer a good quantum number, the selection rules are weakened. What is a cycling transition at small

B-fields develops a leak at larger B-fields allowing decay to other levels. Consequently, the number of atoms participating in the process is reduced and the fluorescence decreases accordingly. The break-up of a cycling transition at larger B-field has been observed in Rb [27].

Furthermore, the number of absorption and emission cycles (and hence, the fluorescence yield) will also decrease as the Zeeman splitting increases with B. When a photon is absorbed from a M_g ground state magnetic sublevel, the fluorescence will bring the population back to M_g or to $M_g \pm 1$ sublevels. When the Zeeman shift of the transition frequency exceeds the homogeneous absorption linewidth, atoms in $M_g \pm 1$ no longer in resonance. Thus at high B-fields Zeeman splitting allows depopulation pumping.

7 Conclusions

We have studied the response of Cs atomic vapor driven by intense linearly- or circularly polarized resonant continuous laser radiation with a frequency near the D_2 transition. Optical pumping drives the population to the $M_g = 0$ or one of the $|M_g| = F_g$ magnetic substates which are the M_g-states with the highest absorption probability. When a B-field induces coupling between M-states (Larmor precession) the consequences of optical pumping are undone and the absorption or the intensity of the fluorescence is reduced. For excitation with circularly polarized light the variation of the signal with B is larger than for excitation with linear polarization. Therefore insertion of a quarter-wave plate into the path of a linearly polarized laser beam may increase the absorption and fluorescence by up to 29%. The experimental results are faithfully reproduced by density matrix calculations which include the dominant excitation paths.

The authors acknowledge valuable discussions with R.G. Unanyan. A.V.P. and M.A. thank the Deutsche Forschungsgemeinschaft for support of their stay at Kaiserslautern University where the experiment and the simulation of the resonance signals were done.

References

1. G. Moruzzi, F. Strumia, *Hanle Effect and Level-Crossing Spectroscopy* (Plenum Press, New York, London, 1991)
2. E.B. Alexandrov, M.P. Chaika, G.I. Khvostenko, *Interference of Atomic States* (Springer Verlag, New York, 1993), p. 254
3. G. Alzetta, A. Gozzini, L. Moi, G. Orrioli, Nuovo Cim. B **36**, 5 (1976)
4. E. Arimondo, Progr. Opt. **35**, 257 (1996)
5. M. Scully, S.-Y. Zhu, A. Gavrielides, Phys. Rev. Lett. **62**, 2813 (1989)
6. M. Scully, M. Fleischhauer, Phys. Rev. Lett. **69**, 1360 (1992)
7. A. Aspect, E. Arimondo, R. Kaiser, N. Vansteenkiste, C. Cohen-Tannoudji, Phys. Rev. Lett. **61**, 826 (1988)
8. S. Harris, Phys. Today 36 (July 1997)
9. D.F. Philips, A. Fleischhauer, A. Mair, R.L. Walsworth, M.D. Lukin, Phys. Rev. Lett. **86**, 783 (2001)
10. C. Liu, Z. Dutton, C.H. Behroozi, L.V. Hau, Nature **409**, 490 (2001)
11. F. Renzoni, A. Lindner, E. Arimondo, Phys. Rev. A **60**, 450 (1999)
12. F. Renzoni, W. Maichen, L. Windholz, E. Arimondo, Phys. Rev. A **55**, 3710 (1997)
13. Y. Dancheva, G. Alzetta, S. Cartalava, M. Taslakov, Ch. Andreeva, Opt. Commun. **178**, 103 (2000)
14. G. Alzetta, S. Cartaleva, Y. Dancheva, Ch. Andreeva, S. Gozzini, L. Botti, A. Rossi, J. Opt. B: Quant. Semiclass. Opt. **3**, 181 (2001)
15. F. Renzoni, C. Zimmermann, P. Verkerk, E. Arimondo, J. Opt. B: Quant. Semiclass. Opt. **3,** S7 (2001)
16. F. Renzoni, S. Cartaleva, G. Alzetta, E. Arimondo, Phys. Rev. A **63**, 065401 (2001)
17. J. Alnis, M. Auzinsh, J. Phys. B **34**, 3889 (2001)
18. A.M. Akulshin, S. Barreiro, A. Lezama, Phys. Rev. A **57**, 2996 (1998)
19. A. Lezama, S. Barreiro, A.M. Akulshin, Phys. Rev. A **59**, 4732 (1999)
20. R. Wynands, A. Nagel, S. Brandt, D. Meschede, A. Weis, Phys. Rev. A **58**, 196 (1998)
21. W.M. Klipstein, S.K. Lamoreaux, E.N. Fortson, Phys. Rev. Lett. **76**, 2266 (1996)
22. W. Happer, Rev. Mod. Phys. **44**, 169 (1972)
23. A.P. Kazantsev, V.S. Smirnov, A.M. Tumaikin, I.A. Yagofarov, Opt. Spectrosc. (USSR) **57**, 116 (1984)
24. R.N. Zare, *Angular Momentum, Understanding Spatial Aspects in Chemistry and Physics* (J. Wiley and Sons, New York, 1988), p. 250
25. A.V. Taichenachev, A.M. Tumaikin, V.I. Yudin, JETP **83**, 949 (1996)
26. M. Auzinsh, R. Ferber, *Optical Polarization of Molecules* (Cambridge University Press, Cambridge UK, 1995), p. 305
27. J. Alnis, M. Auzinsh, Phys. Rev. A **63**, 023407 (2001)
28. I.I. Sobelman, *Atomic Spectra and Radiative Transitions* (SpringerVerlag, Berlin, 1979), p. 359
29. M.P. Auzinsh, R.S. Ferber, Phys. Rev. A **43**, 2374 (1991)
30. M.P. Auzinsh, R.S. Ferber, Sov. Phys. Usp. **33**, 833 (1990)
31. M.P. Auzinsh, R.S. Ferber, Opt. Spectrosc. (USSR) **55**, 674 (1983)
32. E. Arimondo, M. Inguscio, P. Violino, Rev. Mod. Phys. **49**, 31 (1977)
33. C.E. Theodosiou, Phys. Rev. A **30**, 2881 (1984)